Materials Characterization 114 (2016) 103–114

Contents lists available at ScienceDirect

Materials Characterization

journal homepage: www.elsevier.com/locate/matchar

The effectiveness of combining rolling deformation with Wire–Arc Additive Manufacture on β-grain refinement and texture modification in Ti–6Al–4V

J. Donoghue [a,*], A.A. Antonysamy [a,1], F. Martina [b], P.A. Colegrove [b], S.W. Williams [b], P.B. Prangnell [a]

[a] School of Materials, University of Manchester, Manchester M13 9PL, UK
[b] The Welding Engineering Research Centre, Cranfield University, Bedfordshire MK43 0AL, UK

ARTICLE INFO

Article history:
Received 15 October 2015
Received in revised form 4 January 2016
Accepted 6 February 2016
Available online 8 February 2016

Keywords:
Additive Manufacture
Titanium
Grain structure
Texture,

ABSTRACT

In Additive Manufacture (AM), with the widely used titanium alloy Ti–6Al–4V, the solidification conditions typically result in undesirable, coarse-columnar, primary β grain structures. This can result in a strong texture and mechanical anisotropy in AM components. Here, we have investigated the efficacy of a new approach to promote β grain refinement in Wire–Arc Additive Manufacture (WAAM) of large scale parts, which combines a rolling step sequentially with layer deposition. It has been found that when applied in-process, to each added layer, only a surprisingly low level of deformation is required to greatly reduce the β grain size. From EBSD analysis of the rolling strain distribution in each layer and reconstruction of the prior β grain structure, it has been demonstrated that the normally coarse centimetre scale columnar β grain structure could be refined down to <100 μm. Moreover, in the process both the β and α phase textures were substantially weakened to close to random. It is postulated that the deformation step causes new β orientations to develop, through local heterogeneities in the deformation structure, which act as nuclei during the α → β transformation that occurs as each layer is re-heated by the subsequent deposition pass.

1. Introduction

Near-net-shape fabrication of metallic components by Additive Manufacture (AM) is an important new technological area with many potential applications in the aerospace industry (e.g. [1–17]). AM involves building parts by sequentially consolidating 2D slices of material that are fused together by a focused heat source [1–3]. A range of AM processes are now available, mainly based on laser or electron beam systems, that use powder or wire feedstock [1–12]. Of these techniques, powder bed methods allow more geometrically complex components to be produced, but the part size is restricted by slow build rates and the limited dimensions of the working chamber [1–4].

Recently, a low cost wire-based AM process that exploits standard welding technology has become of interest to industry [9–11]. In Wire–Arc Additive Manufacture (WAAM) a consumable wire is fed at a controlled rate into an adapted electric arc (or plasma) welding torch that is translated by a robot [9–12]. Material is built up in the form of a weld bead that is overlaid on previously deposited tracks. Shielding can be provided by an inert gas flooded hood, or deposition can take place in an atmospherically controlled chamber. The WAAM process has a much higher deposition rate than most other metal additive manufacturing techniques (up to 10 kg/h). It also provides better material utilization than powder based methods [9–12], but is restricted to wider wall thicknesses and cannot produce as fine scale features. This low cost process is therefore most suited to producing larger scale parts with less complex geometries.

The α–β titanium alloy, Ti–6Al–4V, is the 'work horse' of the aerospace industry and widely used in airframe and aeroengine applications, where the production of near-net shape components by AM can result in significant cost savings. However, a current concern with AM using this alloy is that coarse primary columnar β grain structures are nearly always observed to be produced in the consolidated material. This undesirable grain structure is seen across a wide range of AM platforms [6, 9–16]. With wire based AM the primary β grains are often as tall as the build height and with larger components can be tens of centimetres long [9–16]. This strong tendency to form coarse-columnar β grain structures in AM with Ti–6Al–4V is difficult to avoid because it results from a combination of the solidification conditions in a small heated moving melt pool, where there is a steep positive thermal gradient at the solidification front, and the metallurgical characteristics of the alloy itself [13–16]. In particular, the Ti–6Al–4V alloy system does not

* Corresponding author.
E-mail addresses: jack.donoghue@manchester.ac.uk (J. Donoghue), alphons.antonysamy@gknaerospace.com (A.A. Antonysamy), f.martina@cranfield.ac.uk (F. Martina), p.colegrove@cranfield.ac.uk (P.A. Colegrove), s.williams@cranfield.ac.uk (S.W. Williams), philip.prangnell@manchester.ac.uk (P.B. Prangnell).
[1] Now at GKN Aerospace, PO Box 500, Golf Course Lane, Filton BS34 9AU, UK.

http://dx.doi.org/10.1016/j.matchar.2016.02.001
1044-5803/

lend itself to nucleation ahead of the solidification front because of the high partition coefficients of aluminium and vanadium, which are close to one, and the lack of suitable grain refining particles in the melt [17]. These process and metallurgical limitations restrict the degree of constitutional supercooling that can occur so that, when combined with a lack of melt inoculants, nucleation ahead of the solidification front is difficult to achieve [13–16].

Although in AM the β grain structure developed during solidification transforms to a fine α and retained β lamellar structure on cooling below the β-transus temperature, the microstructural memory of the coarse, directional, primary-β microstructure can still have a significant impact on mechanical performance. In particular, directional growth of large primary β grains generally produces a strong <001> fibre texture, which gives rise to a related α transformation texture [13–16] and this can potentially result in texture clustering of aligned α-plates within the β matrix. Such factors are known to be detrimental to fatigue life [18, 19] and can contribute to mechanical anisotropy [20–22]. In addition, with a coarse primary β grain structure, grain boundary α can cause premature failure in transverse loading [21, 23]. However, to date, little systematic work has been published on the texture found in AM titanium components produced by wire-based techniques like the WAAM process.

Potential methods for refining the poor primary grain structure seen in AM deposits include; i) modification of the solidification conditions in the melt pool, through manipulation of the process variables [10], or ii) altering the alloy chemistry [17, 24, 25]. However, in AM there is limited scope for changing the process window, because this is dictated by the conditions required to obtain stable part dimensions [9, 10]. Furthermore, while trace additions of elements like boron are known to act as growth restrictors in titanium [25] this can have negative consequences through the formation of brittle second phase particles (e.g. TiB).

In the present work an alternative approach has been investigated for improving the large columnar β-grain structures and strong textures typically seen in wire-based AM processes. This has involved the introduction of a small deformation step sequentially with the deposition of each layer. The deformation step was applied using a roller integrated with the AM system, so that each deposited layer could be lightly deformed before adding a new layer of material (Fig. 1). Although this set up limits the technique to simpler geometries, the aim of this approach was to see if it was possible to introduce sufficient plastic deformation into each layer so that refinement of the β-grains could occur during re-heating, when the next layer was deposited. It was also hoped that this might generate a weaker texture, which would lead to more isotropic mechanical properties [18, 19, 26]. Although the introduction of a light rolling step in AM will moderately reduce the rate of build-up of material and causes a slight spreading in the wall width, this can be controlled in an automated manufacturing system and would not be a major issue when building relatively simple component designs. In fact, it has been found that rolling increases the accuracy of the wall dimensions, by correcting variation in the wall width caused by the bead profile [27]. There are also other potential methods available for applying deformation to each layer in AM that are not so restricted by geometry, such as by peening [28]; hence the efficacy of this novel approach is of more general interest.

It should be noted that in this collaborative study the concept of the hybrid WAAM deformation process was developed by Cranfield University Welding Engineering Research Centre [27, 29], who have previously published work investigating the effect rolling has on the residual stress within the builds [27], and noting the effect on the refinement of the microstructure [30]. The current work, performed at Manchester University, is complementary in that it investigates the effect the refinement has on the primary β and final α texture, and goes into more detail than the previously into the mechanism of formation and the distribution of the refined β grain structure.

2. Experimental

2.1. WAAM samples

The undeformed and rolled WAAM samples were built using a Ti–6Al–4V alloy welding wire (1.2 mm diameter) with a titanium base plate of the same alloy. The substrate material was a conventional hot rolled and annealed plate that had a recrystallized equiaxed α–β microstructure [18]. The samples studied were produced under identical conditions — as one meter long, 20 layer high, straight, vertical walls, using a pulsed GTAW welding system with an average current of 110 A. Each

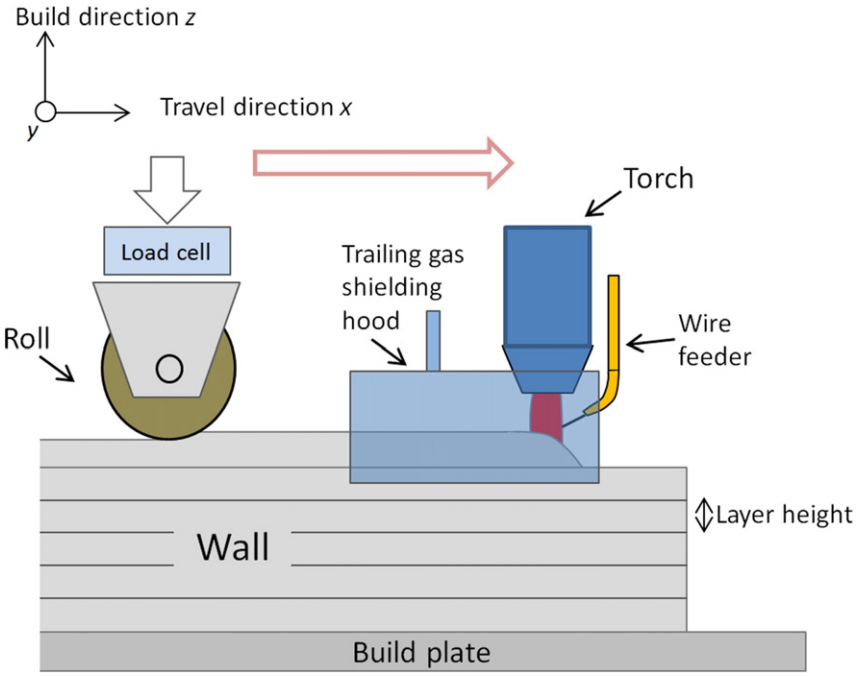

Fig. 1. Schematic diagram of the combined WAAM rolling process.

Table 1
WAAM deposition parameters used to build the walls investigated.

Deposition parameter	Value
Travel speed	270 mm/min
Average arc voltage	12 V
Average current	110 A
Wire feed speed	1.6 m/min
Frequency	10 Hz
Trailing shield gas flow rate	20 l/min

wall was a single track wide and had a width of ~6 mm. Argon shielding was provided by a trailing hood containing a laminar flow device with a high gas flow rate. This resulted in an average oxygen content in the deposited walls of <1500 ppm. The deposition parameters employed are given in Table 1 and full details of the WAAM process can be found in ref [9]. To produce the deformed samples, after deposition of each individual layer, a 100 mm diameter roller was run across the top of the walls using a rigid gantry system on which the welding torch was also mounted (see Fig. 1). Each layer was rolled after the temperature of the top layer cooled naturally to well below 300° (i.e. close to cold deformation conditions and well into the α–β field). The roller employed contained a 3.6 mm radius semi-circular groove, designed to approximately match the curvature of the bead surface. The compressive load during rolling was controlled using a load cell and was applied directly downwards through the roller bearings to the top of each wall.

Five sample conditions were analysed; (i) a control sample built without rolling, as well as two walls to which rolling was applied after adding every layer, with a down-force of (ii) 50 or (iii) 75 kN, and two walls where rolling was only applied to the penultimate layer with the same loads (i.e. (iv) 50 and (v) 75 kN) and the final layer was not deformed.

In the results presented, a standard reference frame has been used for the orientation of all the samples where; *z* is the direction normal to the deposited layers (and parallel to the wall height), *x* is parallel to the wall length and coincident with both the torch travel and rolling direction, and *y* is the transverse direction normal to the wall surface (see Fig. 1). For the samples rolled every layer the net reduction in wall height is given in Table 2, where it can be seen that the 50 and 75 kN rolling loads resulted in an average compressive strain (ε_z) of 8 and 19% respectively.

2.2. Characterisation techniques

The undeformed and rolled AM samples were characterised in two cross-sections for microstructure and textural analysis; i. down their centre line in the vertical *x*–*z* plane and ii. in the plane of the layers (*x*–*y*), half way up each wall — to observe any microstructural variation vertically and through the thickness. Following standard preparation procedures, etching and optical microscopy was used to reveal the deposits' macrostructures. Metallographically prepared samples were analysed by scanning electron microscopy and electron back scatter diffraction (EBSD) orientation mapping using a CamScam Maxim FEG-SEM. Orientation maps were collected with an Oxford instruments EBSD system, with Aztec acquisition software. Large area maps of ~12 × 6 mm, with a 5 μm step size, were used to obtain average texture data and provide comparative macro-views of the coarse β-grain structure across all samples.

Table 2
Change in average layer height and wall width after rolling each added layer in the Ti6Al4V builds, along with the estimated average true principle strains.

Sample	Layer height	Rolling reduction	Wall width	Change in width	ε_z	ε_y	ε_x
Control	1.13	–	5.71	–	–	–	–
50 kN	1.04	0.09	6.17	0.46	−0.083	0.077	0.006
75 kN	0.93 (mm)	0.20 (mm)	6.71 (mm)	1.00 (mm)	−0.19	0.16	0.03

2.3. β-phase reconstruction and texture analysis

In a Ti–6Al–4V alloy with a fine lamellar microstructure it is challenging to index the residual β-phase directly by conventional EBSD because of its small scale and low volume fraction (~5–9% [31]). The high temperature parent β phase grain structures and textures that were originally present after solidification, prior to transformation on cooling, were therefore reconstructed from room temperature α orientation data using a procedure developed by Davies and Wynne [32, 33], based on earlier work by Humbert et al. [34, 35]. Full details of this approach can be found in ref. [32]. The reconstruction procedure uses the Burgers Orientation Relationship (BOR) between the α and β phase to calculate the six possible β parent orientations for each α plate [32–35]; where the BOR is given by:

$$\{100\}\beta//\{0002\}\alpha \quad <111>\beta//<11\bar{2}0>\alpha.$$

The most probable parent β orientation for each α plate is then selected by comparing the most common solution for the misorientations between neighbouring data points. Variables within the procedure that can be altered are the misorientations between neighbouring α points, that can be considered the same α variant, and the allowable maximum angular deviation from the ideal BOR [32]. Here, these parameters were kept at 2° and 3°, respectively.

Texture information was extracted from the original measured α EBSD maps and reconstructed β orientation data and is presented in standard pole figures. In all the orientation maps, inverse pole figure (IPF) colouring has been used with the reference axis aligned with the main fibre direction, which is close to *z*. High angle grain boundaries (HAGBs) >15° in misorientation are depicted by black lines.

2.4. Strain distribution in the AM deposits

In order to relate the plastic deformation to the refined microstructure, it is necessary to map the distribution of the plastic strain as well as the distribution of the grain sizes. Two different approaches were applied to determine the plastic strain distribution in the rolled AM samples using EBSD maps; i) from the pattern quality and ii) the relative effect on the deviation of the misorientation of neighbouring α variants from fulfilling the BOR. If the microscope conditions are kept constant, variation in pattern quality can be attributed to local changes in distortion of the crystal lattice caused by the rolling deformation [36]. The standard measure of pattern quality is Band Contrast (BC), which refers to the brightness of the diffracted bands above background. However, here the Band Slope (BS) was used, which is the gradient of the intensity of signal at the edge of a band (slope of the intensity above back ground). BS was chosen due to the lower sensitivity of the probed volume to crystallographic orientation, compared to BC, which is more strongly affected by how well orientated the crystallographic planes are for diffraction [37]. For method ii) the deviation of misorientations between neighbouring α variants from fulfilling the BOR, within the EBSD data, was determined using the β reconstruction software. In Ti alloys this method is effective because, although there will be local variability between specific α variants, on average the degree of rotation of neighbouring α plates away from the ideal BOR increases with plastic strain [38]. Although neither of the above techniques gives direct values for the strain, they both give a reliable qualitative indication of how the strain is relatively distributed within the wall.

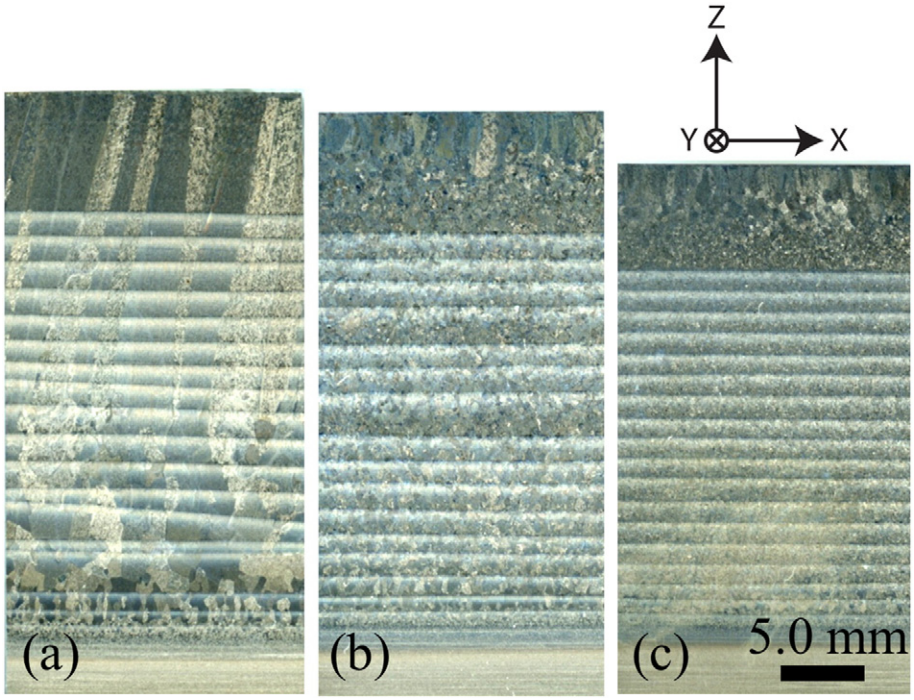

Fig. 2. Macroscopic views of sections through the WAAM walls, cut along their centre, *x*–*z*, plane produced; (a) without deformation and with an increasing applied rolling load, of (b) 50 kN and (c) 75 kN.

3. Results

3.1. Overview

Macroscopic optical images of sections through the centre of the WAAM walls (*x*–*z* plane) produced with and without deformation applied to each added layer, are shown in Fig. 2. The main features that can be noted are the prior β grain structure that developed on solidification, before transformation to an α–β lamellar microstructure on cooling to room temperature, and the regularly spaced horizontal white bands. In the un-rolled wall (Fig. 2a) the presence of very large prior columnar β grains can clearly be seen, which run upwards virtually throughout the entire build height. In comparison, when rolling was applied (Fig. 2a & b), coarse columnar β-grains are absent and the new grain structure is hard to distinguish at this magnification. However, smaller columnar grains can still be observed in the last added layer, which has not been reheated by subsequent deposition passes.

The spacing of the white bands seen in Fig. 2 corresponds to the height of each added layer. The bands are formed within the Heat Affected Zone (HAZ) that developed by the moving thermal field below the heat source, as each new layer is deposited [9]. Similar banding has been seen in other AM processes [6, 9, 12, 15] and is thought to occur at a depth where the peak temperature reached was just below the β transus temperature. This has been reported to result in local coarsening of the transformation microstructure [9, 12]. In most AM processes the thermal field depth that causes this effect corresponds to three to five added layers, depending on the processing conditions [6, 9, 11]. With the WAAM process the first white band can be seen to be at a depth of about 8 mm below the top surface (Fig. 2) and occurred at a depth equivalent to approximately four layers. In the last layer deposited, the newly added and re-melted material solidifies as the β phase and the material within the HAZ of the last pass above the top white band is fully re-heated into the β phase field. This region then transforms directly to α on cooling, although material lower down in the HAZ will have been re-heated and re-transformed between one and three times, depending on the sequential layer number [6]. Hence, the top four layers above the last white band, where deformation was concentrated when each new layer was rolled (see Section 3.2), had a similar fine lamellar transformation microstructure. This microstructure was relatively uniform and was mainly comprised of a Widmanstätten α morphology, with thin layers of retained β between the lath boundaries (Fig. 3). Regardless of being rolled or not, all the samples underwent a very similar cooling rate [30] through the β transus, and therefore the α transformation structure was found to be nearly identical for all build conditions.

3.2. Strain distribution

In Fig. 2 the application of a rolling pass to each added layer can be seen to have reduced the overall height of the walls by an amount that increased with the applied load. The average principal (true) strains implied by the net wall shape change are shown in Table 2. It can be seen that the samples rolled with an applied load of 50 and 75 kN had deformed by an average compressive strain in *z* of 8 and

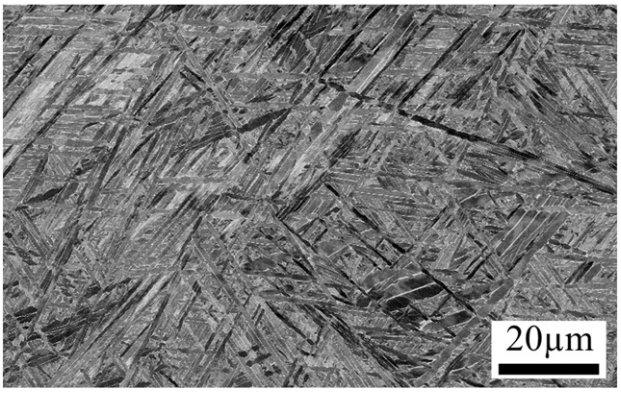

Fig. 3. Example of the typical α–β transformation microstructure seen in the WAAM deposits.

19%, respectively. The net strain values indicate a decrease in average layer height and an increase in wall width after deformation, while the increase in length of the sample along each wall in the rolling direction was relatively small. This is to be expected because, with a thin wall that is attached to a base plate, there is high constraint along the wall in the rolling direction and less lateral constraint than with a conventional rolling geometry. The net average shape change experienced by the WAAM walls was thus close to a plane strain, but with the principal components rotated 90° about the build direction, *z*, (or ND), relative to RD in conventional rolling of a wide plate [39]. However, as will be seen below from the EBSD strain mapping results, the local strain distribution in each layer was found to be highly non-uniform.

The local strain distribution in an individual layer was investigated using the techniques described in section 2.4. In Fig. 4 the change in EBSD pattern quality determined from the band slope (BS) is plotted with depth down the centre line of the walls rolled with 50 and 75 kN loads. It should first be noted that the periodicity observed in the BS plot deeper in each wall (on the right hand side of the plot) is caused by the microstructural banding in the transformation structure described above (Fig. 2). This occurs because local variations in the coarseness of the microstructure within a layer systematically changes the density of α plate boundaries across it, which in turn influences the average value of the BS due to the poorer quality of overlapping diffraction patterns encountered at grain boundaries. In comparison, towards the left side of the graph (i.e. closer to the top wall surface), which is from the region above the last white band seen in each wall, there is little variation in the α microstructure. When this effect is taken into account, the underlying trend in the BS curves can be attributed to the relative plastic strain within the α-phase. For both rolling loads the BS value can be seen to decrease to a minimum below the top wall surface before increasing again to level out at constant value. This behaviour can be interpreted as the plastic strain from rolling being low near the top surface and increasing to a maximum at a depth of between 1.5 and 2.5 mm, before then falling off further down the wall to approach zero at a depth of about 5 and 8 mm, for the 50 and 75 kN loads, respectively. It can be further seen that for the sample produced with a 75 kN rolling load the minimum position in BS value is both deeper and wider than with a 50 kN load; suggesting that, not only the local strain was larger with a greater rolling load, but that the depth where the greatest plastic strain occurred also penetrated further below the rolled surface (2 as opposed to 1.5 mm, with the 75 and 50 kN loads, respectively).

The conclusion that the plastic strain generated by rolling each layer was low at the top surface, and greatest between 1.5 and 2.5 mm deep in each wall, can be attributed to the constraint imposed by the profiled roller. This interpretation can be further corroborated by using the BOR misorientation mapping technique, the results of which are depicted in

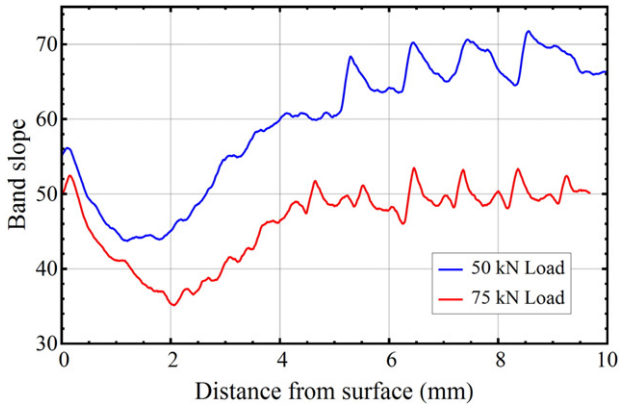

Fig. 4. EBSD pattern quality, measured by the relative band slope, for the two rolled walls plotted with vertical distance down their centre from their top surface.

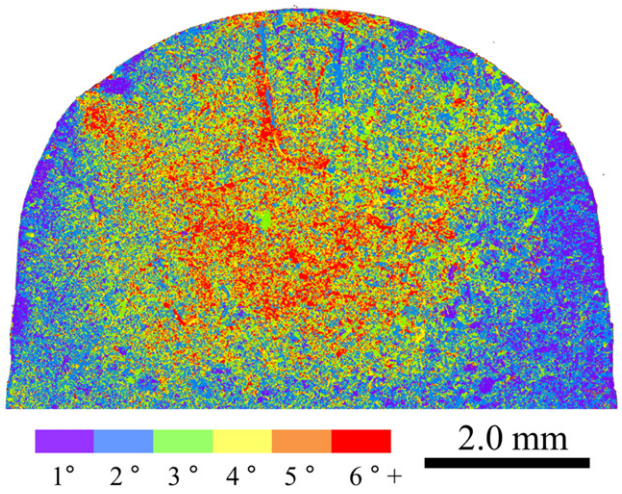

Fig. 5. The strain distribution seen in the top section of the 75 kN rolled wall, inferred by plotting the deviation of neighbouring α laths from fulfilling the ideal Burger's orientation relationship.

Fig. 5. As well as confirming that the maximum strain was concentrated at a specific depth below the top of each rolled wall, the map in Fig. 5 also demonstrates that the strain developed by the grooved roller was not evenly distributed across a wall's width, being focused in its centre with respect to the wall's width.

3.3. Effect of rolling on refinement of the primary β-grain structure

Fig. 6 compares EBSD orientation maps of both the α-phase and reconstructed parent β grain structures seen in the un-rolled control and rolled WAAM walls. The maps depicted are *x*–*z* centre plane cross-sections taken from the top of each wall to a depth of ~10 mm (equivalent to about the last 8 layers). In the α phase EBSD maps (Fig. 6a–c) a memory of the parent β grain structure is evident from the texture clustering seen in the α variants, which is particularly obvious in the un-rolled control sample. However, following reconstruction it becomes very apparent that a coarse columnar β grain structure with a strong texture developed in the un-rolled wall before its transformation to α (Fig. 6d). The red colouring that dominates the β phase in this IPF map indicates that the columnar grains have strong preferential alignment with a mutual <001> fibre [13–16]. In the undeformed wall it can also be seen that the columnar β grains have a width of approximately 2 mm and their lengths' can be measured in centimetres.

In contrast, when the rolling step was applied to each deposited layer, a much more refined equiaxed β-grain structure was observed, as well as a weaker texture (Fig. 6e & f). Greater grain refinement was also seen in the wall that had received a higher rolling load. In Fig. 6e & f it is further apparent from the grain structure that is formed in the last layer, how quickly a columnar structure is re-established when it has not been refined by rolling and re-heating. Finally, a band can be seen in Fig. 6e and f between a depth of 1–4 mm below the rolled wall's top surfaces where there are unindexed points in the maps. These missing points result from data being discounted during β reconstruction because it had too great a deviation from the BOR and the depth of this band coincides with the strain distribution generated by rolling the last layer, as described above (Figs. 4 and 5).

Fig. 7 shows EBSD maps from *y*–*z* transverse wall cross-sections that have been coloured to highlight the size distribution of the refined β grains. In (a) and (b) rolling was only applied to the penultimate layer, and in (c) and (d), as before, every layer was rolled. The images in Fig. 7c and d, therefore, correspond to the transverse sections from the walls previously described in Fig. 6. The grain sizes given are the

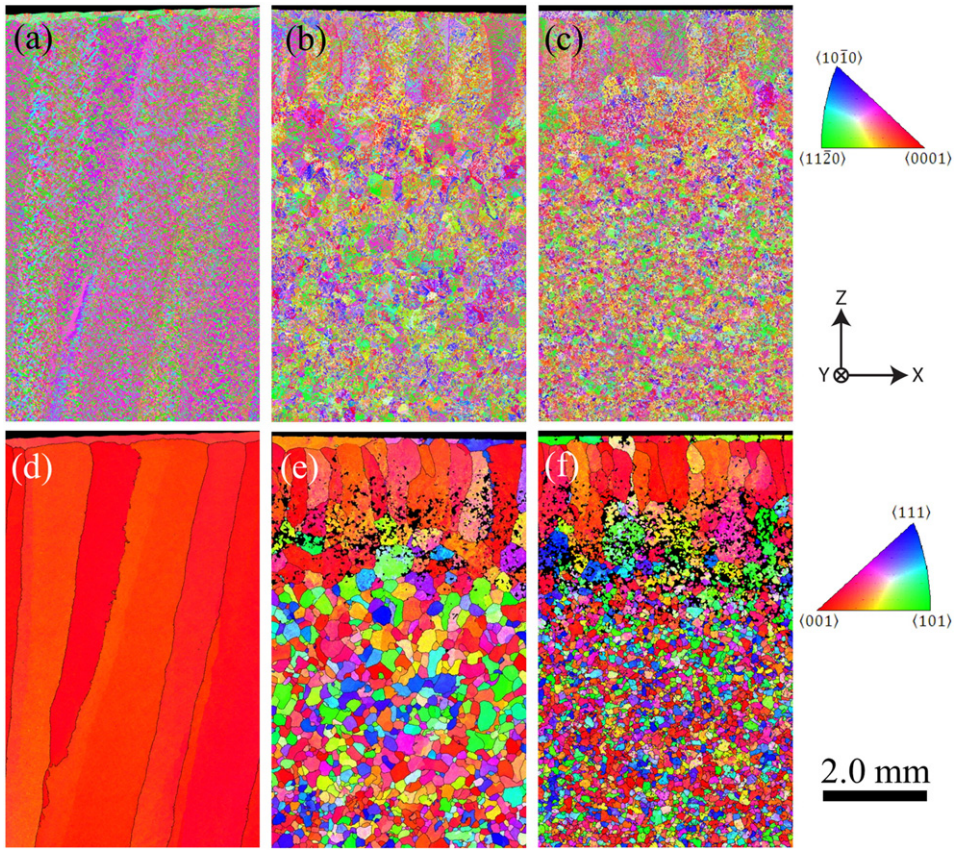

Fig. 6. Measured α-phase (a–c) and reconstructed β-parent phase (*d*–f) IPF orientation coloured EBSD maps from the undeformed control and rolled WAAM walls, produced with rolling loads of 50 and 75 kN, obtained from mid plane, *x*–*z*, wall sections.

equivalent circular diameter of the reconstructed β-grains. From Fig. 7a and b it is evident that when a rolling pass was only applied to the penultimate layer, and it was re-heated during depositing the next and final layer, refinement of the β grain structure predominantly occurred below the top surface within a core region in each wall. This region of β refinement can be seen to increase with rolling load and shows good qualitative agreement with the plastic strain distribution inferred from Fig. 6.

When rolling was applied to every added layer (Fig. 7c & d) the width of the refined core region increased, relative to the samples where only the penultimate layer was rolled (Fig. 7a & b), and extended all the way down each wall. The average grain sizes measured below the top layer across these walls are given in Fig. 8a. With both rolling loads, the grain size can be seen to increase towards each wall's outer surfaces and there is a central plateaus region where the average grain size is refined to a minimum level, which reduces with increasing applied load. In the core region at the centre of the walls the β grain size was reduced to around 140 and 90 μm with rolling loads of 50 and 75 kN, respectively. In addition, with the higher 75 kN load the grain size in the wall core was more uniform and the core region was proportionally wider compared to the wall thickness.

An equivalent plot depicting the variation in grain size with vertical position down the centreline of the rolled wall samples is given in Fig. 8b. The grain size data for both rolling loads shows an increase in average diameter at the top of each wall, which corresponds to the re-establishment of a columnar β structure in the final layer to solidify (Fig. 6e & f). Below this transition region, rolling each layer refined the grain size to a relatively uniform minimum level with the larger 75 kN rolling load, but when the 50 kN downforce was used there was far more variability. A histogram of the grain sizes in the fully refined core region of this cross-section is given in Fig. 9. It should be noted that grain sizes below the reliable measurement limit for the set up used have been excluded (25 μm) from the EBSD data. However, the average grain sizes were found to be 130 μm and 94 μm for the 50 kN and 75 kN rolling loads respectively, which corresponds well with measurements made by the line intercept method on optically acquired micrographs in a previous study [30]. In it is also evident from Fig. 9 that the β grain size distribution from the refined core regions of the rolled walls was more tightly distributed around the smaller mean value when the larger rolling load was used. For example, with a 50 kN down force the largest grain measured 590 μm) was almost twice the size of that observed in the 75 kN sample (350 μm).

3.4. Effect of rolling on texture in the WAAM process

Strong crystallographic textures can cause anisotropy in a material's mechanical properties and this can be particularly pronounced in titanium alloys that have hcp crystal structures [18, 40, 41]. In the undeformed AM wall the reconstructed EBSD map in Fig. 6d clearly indicates the presence of a strong β-texture. However, textural changes can also arise from deformation, or its influence on any recrystallization or phase transformation that may occur during subsequent heat treatment [40, 41]. It is thus important to compare the texture seen in an un-deformed build with that found when a rolling step was utilised with the WAAM process to refine their coarse primary β grain structures.

Pole figures obtained from the large area EBSD maps depicting the α-textures and the reconstructed parent β-textures that existed prior to transformation, on cooling down below the β-transus temperature, are provided in Figs. 10 and 11. The EBSD maps were taken from the centre, *x*–*z*, plane of each wall, and for the rolled walls therefore mainly represent orientations from their more refined core region (Fig. 7). The

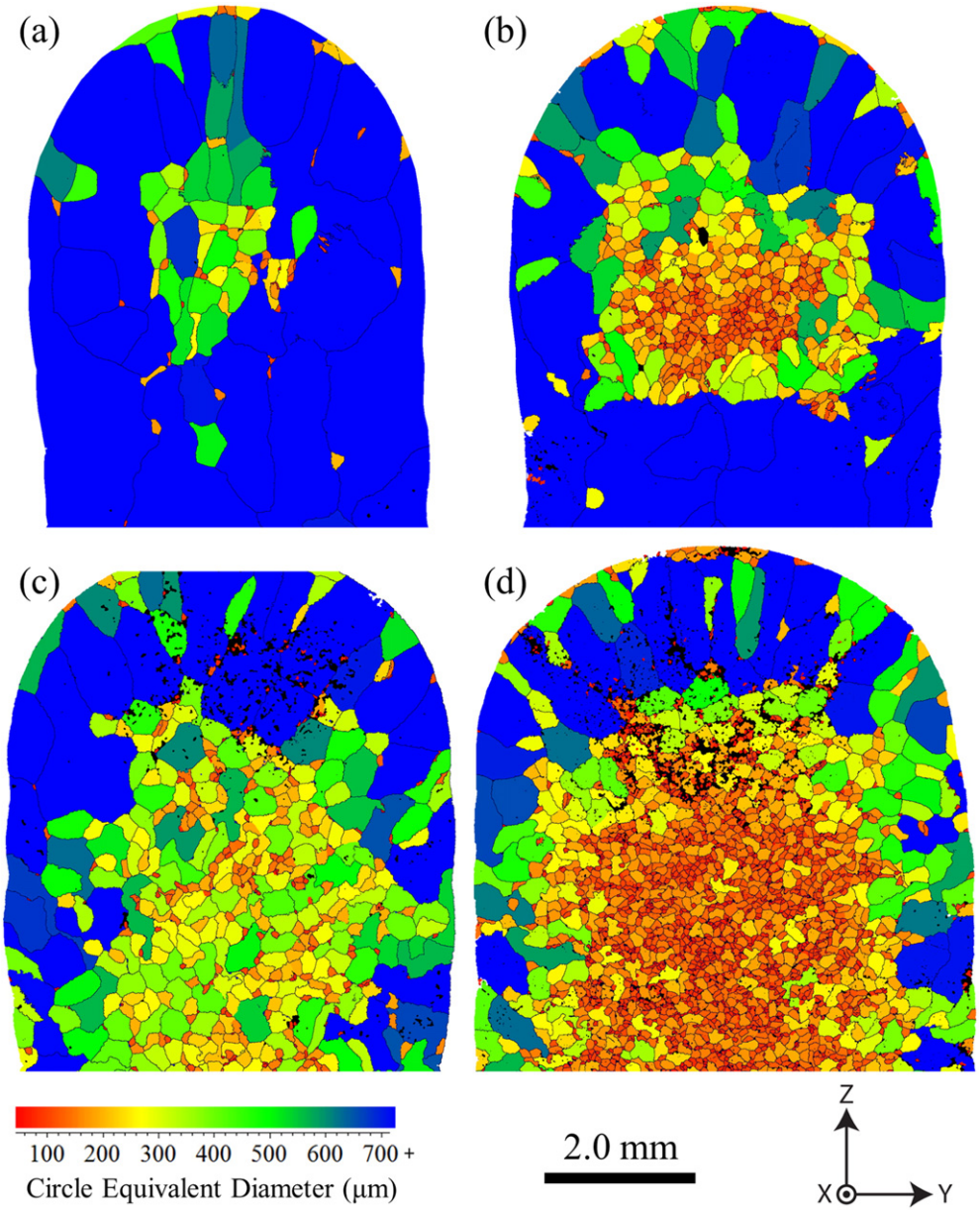

Fig. 7. EBSD reconstructed β grain size maps from transverse, *y*–*z*, cross-sections near the top of rolled WAAM walls; (a) and (b) with *only one* rolling pass applied to the penultimate layer and (c) and (d) with a rolling pass applied to *every* layer, both with rolling loads of 50 kN and 75 kN respectively.

pole figures are orientated with the build direction and compression axis (*z*) near to normal to the plane of projection and the torch travel direction (*x*) is aligned vertically. Before presenting these results it should be noted that the sampling statistics for the solidification texture in the un-deformed wall were poor, owing to the large prior-β grain size (only 10 grains were covered in the map area), whereas the statistics for the textures in the rolled samples were more representative because of their more refined grain structure.

Of the α textures, shown in Fig. 10, the texture of the un-deformed as-deposited wall is difficult to describe at first sight because of the poor β parent grain sampling statistics. However, it becomes much clearer when β phase reconstruction is performed. From the 100 β phase pole figure in Fig. 11a it can be seen that the α phase transformed from β parent grains that had a common <001> direction aligned close to the build direction. The corresponding α-texture seen in Fig. 10a is, therefore, an <001> β transformation texture that is poorly defined, partly because of the poor statistics for the parent β grain orientations, but also because it has become weakened by the twelve possible α variant orientations available through the Burgers relationship [42–44].

In comparison to the strong texture seen in the control sample, much weaker α and β textures were found in the rolled walls (Figs. 10b & c; 11b & c), which had maximum intensities of less than approximately 3 and 4 times random for the α and β phases, respectively. In both of the rolled walls it was found that the strongest orientations present in their reconstructed β pole figures were consistent with the textures containing residual weakened cube components. As can be seen from Fig. 11b and c both the rolled wall's 100 pole figures have one <001> pole aligned close to the build direction, *z*, with the other related <001> poles rotated by different amounts about *z* relative to the deposition direction (e.g. ~10 and 20° in the 50 kN and 75 kN examples shown). These residual <001> fibre orientations were weaker in the wall rolled with a greater down force; the maximum intensity dropping from 3.5 times random for the 50 kN rolling load to 2.8 for the 75 kN load and this led to a corresponding drop in the strength inherited in

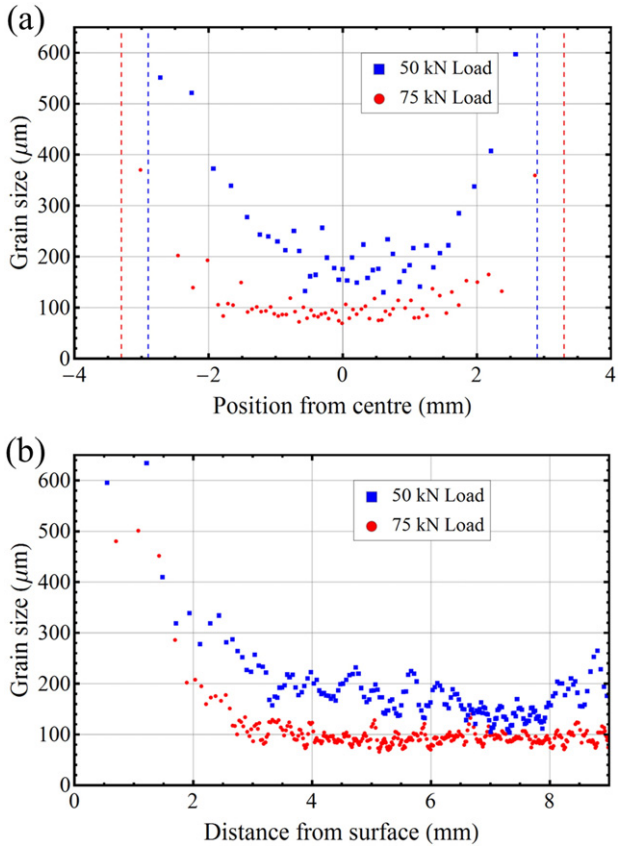

Fig. 8. The average β grain size variation seen in walls produced when every layer was rolled after deposition, with a 50 or 75 kN applied load; (a) across the walls over 5 layers below the final white band and (b) as a function of depth down their centre lines. In (a) the dashed lines indicate the outside surfaces of each wall.

the α transformation textures, on applying rolling to each layer, from 2.7 to 2.2 times random.

4. Discussion

With titanium alloys, coarse-directional grain structures are of concern in the industrial application of AM processes because of their potential to cause anisotropic properties in aerospace components [13, 16, 23]. The above results show that the introduction of a rolling deformation stage sequentially within the WAAM build cycle could be a useful technique for refining such undesirable grain structures, as well as for reducing the intensity of the strong textures normally seen in the as-deposited material. Interestingly, the strain required to achieve a high level of β refinement has been found to be relatively low, which makes it practical to apply such a technology when producing components with relatively simple geometries. However, other methods for introducing plastic deformation in AM are also being investigated, such as peening [28], which offers higher compatibility with more complex component designs.

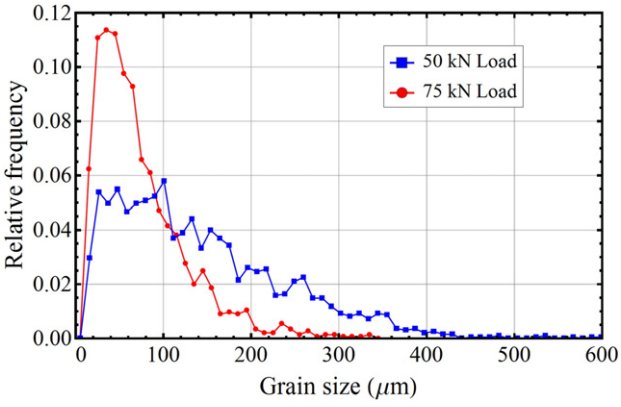

Fig. 9. Comparison of the β grain size distributions measured from reconstructed EBSD maps obtained at the centre of the walls rolled with a load of 50 kN and 75 kN.

4.1. Grain structure development in the conventional WAAM material

By reconstruction of the parent β phase that forms on solidification, it has been confirmed that in the conventional WAAM process a very coarse primary columnar grain structure is developed as material is built up, by sequentially adding many new layers. This columnar grain structure has a strong preferential <001> β texture. It has been previously noted that the main reason such a coarse grain structure develops is because the high thermal gradient in the melt pool and the alloy chemistry do not allow sufficient constitutional supercooling for nucleation to be possible ahead of the solidification front [17]. Similar to welding, in AM when a layer is added the temperature rapidly increases below the fusion boundary and the material high in the heat affected zone will fully transform back to the β phase, whereupon grain coarsening will occur where the peak temperature reached is significantly above the β transus [11] (Fig. 6d). When solidification of the single β phase subsequently takes place at the rear of the moving melt pool, because nucleation ahead of the growth front is not possible, the coarsened β-grains at the fusion boundary then act as a substrate for epitaxial re-growth back into the liquid following the maximum thermal gradient, which is normal to the solidification front. A columnar structure is thus developed as grains grow following the rear melt pool surface [45].

This process repeats as more layers are added, with the retained β in the transformation microstructure re-growing, each time when it is re-heated in each new cycle to re-create β grains with the same orientation they had in the previous pass. When re-heated above the β transus, the reformed β grains can also potentially coarsen each cycle, before providing the substrate for epitaxial re-growth at each new fusion boundary. Hence, in AM without deformation the same grain orientations re-grow over may layers as each new layer is added. As the β-grains develop, grain growth thus occurs both in the solid state and during solidification where orientations are progressively selected that have a preferred <001> crystallographic direction parallel to the maximum thermal gradient at the solidification front [45], leading to the strong <001> texture seen in the final wall [13–16] (Figs. 5d, 11a). One of the reasons a deformation step is so effective in causing β grain refinement and a weaker texture in AM is thus because it has the potential to disrupt the accumulative 'ratcheting' effect of this repeated cyclic behaviour that is inherent in an additive 'layer' manufacturing process.

4.2. Grain refinement in the rolled WAAM deposits

In the samples studied, the rolling loads employed led to relatively modest average compressive plastic strains of 8 and 19%. Nevertheless, when each deposited layer was sequentially rolled during the AM process, the original coarse columnar grain structure was found to become greatly refined, giving rise to an equiaxed β-grain structure with an average diameter of <100 μm in the core of the wall produced with the 75 kN rolling load. Although the refined β grain size increased towards the surface of the walls, this overall reduction in grain size still compares very favourably to the centimetre-scale columnar grains seen in standard un-deformed samples (Fig. 2). In addition, both the parent β and α phase texture strengths was substantially weakened in the rolled samples.

The refined β grains were formed at temperatures well above the β transus temperature. This is cleary apparent from comparison of Fig. 2 with the refined region in Fig. 7b. In Fig. 2 the top white bands occur

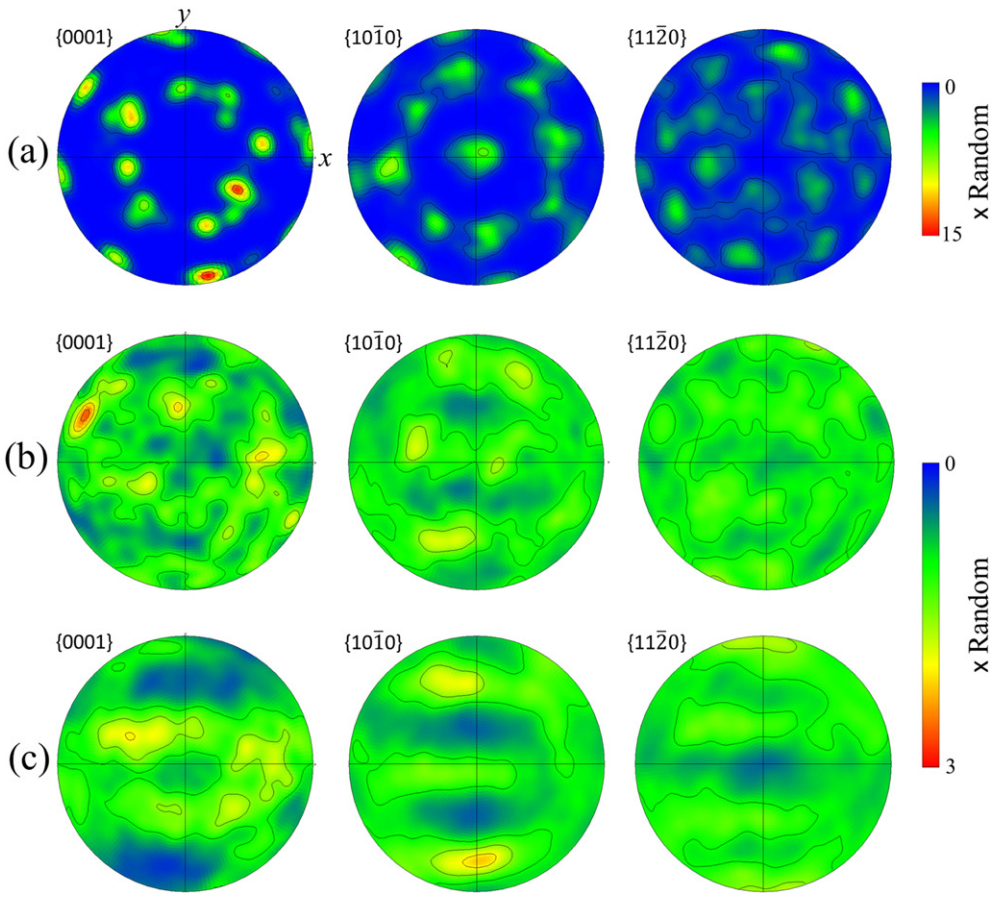

Fig. 10. Pole figures obtained from large area EBSD maps depicting α textures measured from the centre of; (a) the un-rolled wall, (b) the wall rolled with a 50 kN load, and (c) the wall rolled with a 75 kN load.

where the maximum temperature reached in the last pass was just below the β tranus temperature (as has been widely acknowledged [6]) and this is at a depth of over 8 mm's below the top surface which is well below the depth where β refinement occurs in Fig. 7b. In addition, refinement in the β phase would not be expected through conventional recrystallization as the driving force is usually insufficient at such low strain levels of below 20% [46]. It can therefore be concluded that the grain refinement seen at these low applied strains is caused by the growth of new β orientations associated with the influence of deformation on the α → β phase transformation, which occurs during re-heating above the β transus temperature, when the next layer is deposited. This implies rolling creates new β orientations, other than those retained from the parent β grains in the original transformation structure formed during cooling each solidified layer. These orientations can then act as new nuclei that grow on re-heating each layer above the β transus temperature when the next layer is added. This prevents the original β grains simply re-growing the orientations of the substrate during epitaxial solidification of the next layer deposited, which leads to the coarse columnar structures normally seen in undeformed WAAM walls, by the 'ratcheting process' discussed above.

Because the strain applied to each deposited layer was relatively low, the origin of the new β orientations is most probably related to heterogeneities that develop within the deformation of the fine Widmanstätten transformation microstructure found in AM titanium parts. One possible mechanism, already discussed by the current authors in Ref [47], has been observed directly using in-situ heating experiments and involves new β orientations originating from deformation twinning of α laths within the deformed region below the top of a rolled wall. Further related mechanisms, by which new β orientations can be generated by the application of relatively low levels of plastic deformation in AM, also associated with deformation twinning, and from strain concentration at colony boundaries, are still under investigation and will be the subject of a future publication.

EBSD strain mapping has shown that the core wall region where β grain refinement was found to be closely related to the local strain distribution generated in each rolling pass (Fig. 5). This is strongly influenced by the shape of the roller which was profiled to match the curvature of the top layer bead profile. With a grooved roller, the top of the wall is highly constrained and cannot spread sideways, which causes a 'dead-zone' near the roll surface and forces the plastic deformation to be concentrated at a greater depth within the wall core. Although this strain distribution was not pre-planned, it is beneficial when trying to combine deformation with AM techniques like the WAAM process that features a large re-melt depth (~1.5 mm) as it means that the majority of useful deformation is not lost by the deformed material being re-melted by the subsequent pass. Other techniques, such as peening, tend to concentrate plastic deformation closer to a surface [48] and would therefore be less suitable for refining the grain structure unless they are combined with an AM technique that has a low re-melt depth [28].

A negative effect of the grooved roller is that the strain introduced is lower near the wall faces, which leads to a more refined core with coarse grains towards each wall edge. However, when rolling was applied to every added layer (Fig. 7c & d) the width of the refined core region was found to increase and the grain size in the less refined skin was still much smaller than in the undeformed wall. The fact that rolling each layer was more effective than rolling a single layer, is discussed further below and can be explained partly by the fact that repeatedly

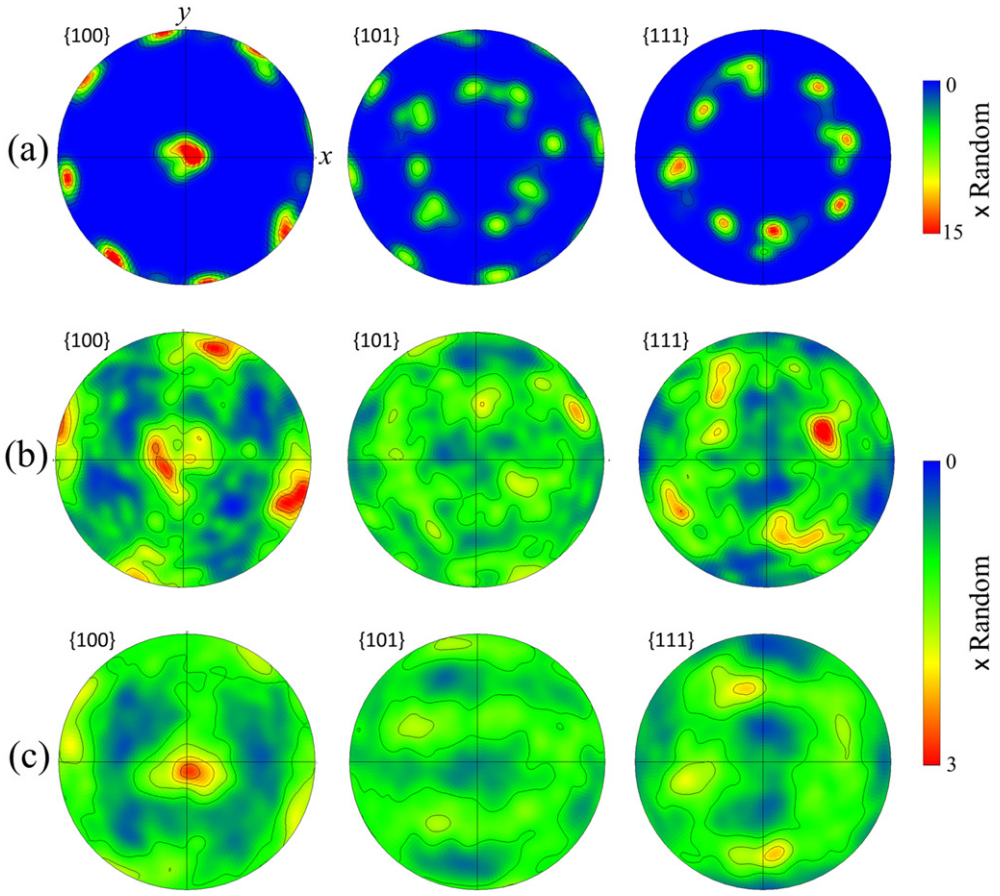

Fig. 11. Pole figures obtained from large area EBSD maps depicting the parent phase β textures reconstructed from the centre of; (a) the un-rolled wall, (b) the wall rolled with a 50 kN load, and (c) the wall rolled with a 75 kN load.

rolling each layer does not allow a coarse β structure to develop, prior to the application of an individual rolling pass, and partly because deformation occurs to a sufficient depth that there is some overlap with the previous layer, which will therefore be deformed and re-heated above the β transus more than once when rolling is applied in every pass.

Apart from in the last added layer, which is not re-heated following deformation, it was found that there was very little variation in grain size with build height for the wall deformed with a 75 kN rolling load every pass. However, more variation was observed in the 50 kN wall (Fig. 8b). The cause of this variation can be related to the lower depth of deformation and greater inconsistency in the deposition conditions that led to more irregularity in the layer height with this sample, as can be observed from the greater unevenness in the vertical spacing of the white bands seen in the 50 kN wall as opposed to the 75 kN sample (Fig. 2). Furthermore, in Fig. 12 it can be noted that there is a clear correlation between the white band layer-thickness and the average refined grain size. It is apparent that a lower rolling load is likely to exaggerate such variability, because there is a lower penetration depth of the plastic strain in each layer; i.e. where there is a narrower, or wider, layer separation this will lead to a finer, or coarser, β grain size because of the greater variation in strain overlap between deformation passes with a lower rolling load.

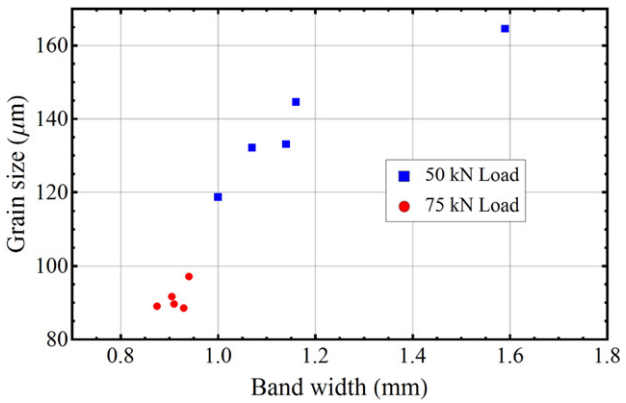

Fig. 12. Average grain size plotted against layer height for the two rolling loads.

4.3. Texture development

The observation of a strong <100> β fibre texture in the un-rolled walls has been discussed above (section 4.1) and is consistent with studies performed with other AM techniques [11, 14]. In the 100 pole figure in Fig. 11a the main fibre axis can be seen to have an intensity of 15 times random, although this value should be treated with cautions as, despite the large area mapped (12 by 6 mm), the prior β grain size was so large sufficient data could not be obtained to develop a full texture description (Figs. 10a and 11a). Owing to the poor sampling statistics, an attempt has therefore not been made to evaluate the possibility of variant selection affecting the α-texture. However, it is interesting that in a recent paper Sargent et al. [31] have claimed that transformation strains can cause variant selection within similarly coarse grains found in Ti–6Al–4V castings. Encouragingly, the application of a deformation step to each layer greatly weakened the β parent textures, to

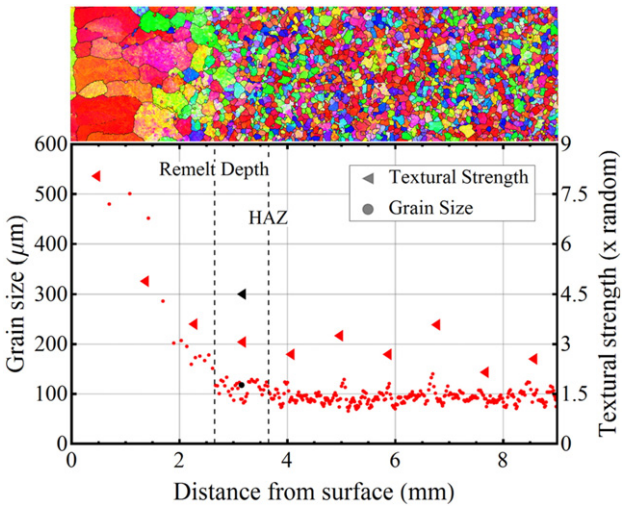

Fig. 13. Plot of β textural strength (given by the maximum intensity in the 100 pole figure) and grain size variation with height down the centre line, for the wall rolled with a load of 75 kN applied to every added layer. Also indicated in blue are the values for the corresponding region in the sample produced with only one 75 kN rolling pass applied to the penultimate layer. The magnified insert is of the β grain structure in top 9 layers of the wall.

3.5 and 2.8 times random with the 50 kN and 75 kN rolling loads, respectively. On transformation this was further diluted leading to extremely weak α textures being seen in the rolled samples of 2.7 and 2.2 times random. Although the maximum intensities were greatly reduced, both of the rolled walls still retained a memory of the original β phase <001> fibre texture that tended to be present as a weaker rotated cube orientations. Overall this suggests that the presence of these components is caused by insufficient sampling statistics, which resulted in a tendency for orientations related to one dominant 'harder' parent β grain, that was more resistant to refinement, to be retained from the original <001> fibre within each EBSD map area.

Finally, the synergistic advantages of applying a rolling step to each layer after it is deposited are highlighted in Fig. 13, which compares the grain size and texture strength down the centre of the wall rolled with the higher load, from its top surface, with an enlarged EBSD map of the same region. In the last layer to be added it can be seen that there is a rapid increase in the β grain size and texture strength towards the top surface of the deposit. It can be noted that this is partly caused by β grain growth in the HAZ below the melt pool, and then is further enhanced by <001> growth selection during the development of a columnar structure by directional solidification. However, in this single layer the grain size reached and texture strength are nowhere near as high as that developed in the un-deformed wall, where the grain size and intensity of the <001> fibre progressively increase through the 'ratcheting' of these two effects during the addition of further layers as a wall is built. This is because when each layer is sequentially rolled the development of a columnar grain structure and strong fibre texture is disrupted after every layer is deposited, and does not have the same opportunity to develop during multiple repeated cycles.

Of additional significance to the synergistic benefit of rolling every layer is that each layer will have a finer grain size and weaker texture before it is rolled than in an unrolled wall, where the columnar structure is much more developed. The single data points shown in Fig. 13, taken from the rolled refined region of the sample where rolling was applied only to the penultimate layer, of an otherwise undeformed wall (Fig. 7b), demonstrate that, in this case the level of grain refinement in the deformed core region is similar, but the resultant texture is much stronger (4.5 as opposed to 2.7 times random) than when the starting microstructure has been previously refined; i.e. when a single rolling pass was applied to a coarse grained undeformed columnar structure, following re-heating by adding the next layer, the grain size refinement was approximately the same as when you start with a refined grain structure, but the reduction in texture strength was still far less. This is because when you start with a stronger texture, that has been able to develop over many layers of β grain growth in an unrolled wall, it will require a larger rolling strain to reduce it to the same level.

Therefore, the addition of a rolling pass to every layer leads to a weak texture in the wall by both preventing the formation of a strongly textured columnar grain structure, which requires many layers of undisturbed growth to develop, and by this, in turn, ensuring a far weaker texture in the next layer before it is deformed. The combination of these two effects thus greatly decreases the rolling strain required to reduce the texture strength in a WAAM component.

5. Conclusions

The efficacy of a deformation step, on refining the primary β grain structure and texture developed in a Ti–6Al–4V alloy, has been investigated during Wire–Arc Additive Manufacture (WAAM). By reconstruction of the β parent phase, from α phase EBSD maps, it has been confirmed that in the conventional WAAM process the deposited material develops centimetre-scale, coarse-columnar, β grains that grow through the build height with an associated strong <001> β fibre texture. This coarse grain structure results from the retained β in the transformation structure re-growing with the same orientations when heated above the β transus, with the next new layer added. Once reformed, the β grains coarsen and act as a substrate for epitaxial columnar growth during solidification of the new layer.

The application of a rolling step sequentially to each added layer was surprisingly effective, in terms of the low level of strain required, to both refine the β grain size and weaken the primary β and final α textures, which were reduced to close to random by the application of an only modest 8–20% rolling reduction. However, the homogeneity of the refined β grains was found to improve with increased levels of deformation. A profiled roller has also been shown to be advantageous for increasing the depth of deformation in each layer — thus helping the deformed region to survive re-melting in the next addition cycle.

It is postulated that the deformation step causes β grain refinement through promoting twinning, which generates new β orientations that then grow during the α → β transformation as each layer is re-heated by the subsequent deposition pass.

There are synergistic advantages of rolling each layer because this disrupts the establishment of the coarse columnar grain structure that only normally develops over many undisturbed repeated addition cycles. Rolling each layer also ensures that the β grain structure is refined and the texture weaker in each new added layer, before it is deformed, and this decreases the deformation required to obtained a weaker texture.

Acknowledgements

The authors would like to thank Prof. Brad Wynne (University of Sheffield) for provision of the β reconstruction software. J. Donoghue is grateful for financial support provided by LATEST2 (EP/H020047/1) and Airbus, UK.

References

[1] I. Gibson, D.W. Rosen, B. Stucker, Additive Manufacturing Technologies, Springer US, Boston, MA, 2010.
[2] J. Kruth, M. Leu, T. Nakagawa, Progress in additive manufacturing and rapid prototyping, CIRP Ann. Technol. 47 (1998) 525–540.
[3] P. Kobryn, N. Ontko, L. Perkins, J. Tiley, Additive Manufacturing of Aerospace Alloys for Aircraft Structures, 2006 2–12.
[4] E.O. Ezugwu, Z.M. Wang, Titanium alloys and their machinability — a review, J Mater Process Technol 68 (1997) 262–274.
[5] X. Wu, J. Liang, J. Mei, C. Mitchell, P.S. Goodwin, W. Voice, Microstructures of laser-deposited Ti–6Al–4V, Mater. Des. 25 (2004) 137–144.

[6] S.M. Kelly, S.L. Kampe, Microstructural evolution in laser-deposited multilayer Ti–6Al–4V builds : part I, Microstruct. Character. 35 (2004) 1861–1867.
[7] S. Kelly, S. Kampe, Microstructural evolution in laser-deposited multilayer Ti–6Al–4V builds: part II. Thermal modeling, Metall. Mater. Trans. A 35 (2004) 1869–1879.
[8] F. Wang, J. Mei, X. Wu, Microstructure study of direct laser fabricated Ti alloys using powder and wire, Appl. Surf. Sci. 253 (2006) 1424–1430.
[9] F. Martina, J. Mehnen, S.W. Williams, P. Colegrove, F. Wang, Investigation of the benefits of plasma deposition for the additive layer manufacture of Ti–6Al–4V, J. Mater. Process Technol. 212 (2012) 1377–1386.
[10] F. Wang, S. Williams, M. Rush, Morphology investigation on direct current pulsed gas tungsten arc welded additive layer manufactured Ti6Al4V alloy, Int. J. Adv. Manuf. Technol. 57 (2011) 597–603.
[11] F. Wang, S. Williams, P. Colegrove, A.A. Antonysamy, Microstructure and mechanical properties of wire and arc additive manufactured Ti–6Al–4V, Metall. Mater. Trans. A 44 (2012) 968–977.
[12] E. Brandl, A. Schoberth, C. Leyens, Morphology, microstructure, and hardness of titanium (Ti–6Al–4V) blocks deposited by wire-feed additive layer manufacturing (ALM), Mater. Sci. Eng. A 532 (2012) 295–307.
[13] A.A. Antonysamy, P.B. Prangnell, J. Meyer, Effect of wall thickness transitions on texture and grain structure in additive layer manufacture (ALM) of Ti–6Al–4V, Mater. Sci. Forum 706-709 (2012) 205–210.
[14] S.S. Al-Bermani, M.L. Blackmore, W. Zhang, I. Todd, The origin of microstructural diversity, texture, and mechanical properties in electron beam melted Ti–6Al–4V, Metall. Mater. Trans. A 41 (2010) 3422–3434.
[15] P. Kobryn, S. Semiatin, Microstructure and texture evolution during solidification processing of Ti–6Al–4V, J. Mater Process. Technol. 135 (2003) 330–339.
[16] A.A. Antonysamy, Microstructure, Texture and Mechanical Property Evolution during Additive Manufacturing of Ti6Al4V Alloy for Aerospace Applications, University of Manchester, 2012.
[17] M.J. Bermingham, S.D. McDonald, M.S. Dargusch, D.H. StJohn, Grain-refinement mechanisms in titanium alloys, J. Mater. Res. 23 (2011) 97–104.
[18] G. Lütjering, J.C. Williams, Titanium, Springer, Berlin Heidelberg, Berlin, Heidelberg, 2007.
[19] I. Bantounas, D. Dye, T.C. Lindley, The role of microtexture on the faceted fracture morphology in Ti–6Al–4V subjected to high-cycle fatigue, Acta Mater. 58 (2010) 3908–3918.
[20] T. Vilaro, C. Colin, J.D. Bartout, As-fabricated and heat-treated microstructures of the Ti–6Al–4V alloy processed by selective laser melting, Metall. Mater. Trans. A 42 (2011) 3190–3199.
[21] H.K. Rafi, N.V. Karthik, H. Gong, T.L. Starr, B.E. Stucker, Microstructures and mechanical properties of Ti6Al4V parts fabricated by selective laser melting and electron beam melting, J. Mater. Eng. Perform. 22 (2013) 3872–3883.
[22] F. Martina, S.W. Williams, P. Colegrove, Improved microstructure and increased mechanical properties of additive manufacture produced Ti–6Al–4V by interpass cold rolling, SFF Symp. 2013, pp. 490–496.
[23] B.E. Carroll, T.A. Palmer, A.M. Beese, Anisotropic tensile behavior of Ti–6Al–4V components fabricated with directed energy deposition additive manufacturing, Acta Mater. 87 (2015) 309–320.
[24] X. Wu, R. Sharman, J. Mei, W. Voice, Microstructure and properties of a laser fabricated burn-resistant Ti alloy, Mater. Des. 25 (2004) 103–109.
[25] M.J. Bermingham, S.D. McDonald, K. Nogita, D.H.St. John, M.S. Dargusch, Effects of boron on microstructure in cast titanium alloys, Scr. Mater. 59 (2008) 538–541.
[26] B. Baufeld, O. van der Biest, Mechanical properties of Ti–6Al–4V specimens produced by shaped metal deposition, Sci. Technol. Adv. Mater. 10 (2009) 015008.
[27] P. Colegrove, H.E. Coules, J. Fairman, F. Martina, T. Kashoob, H. Mamash, et al., Microstructure and residual stress improvement in wire and arc additively manufactured parts through high-pressure rolling, J. Mater. Process. Technol. 213 (2013) 1782–1791.
[28] J. Donoghue, J. Sidhu, A. Wescott, P. Prangnell, Integration of deformation processing with Additive Manufacture of Ti–6Al–4V components for improved β grain structure and texture, 2015 TMS Annu. Meet. Exhib., Orlando, Florida, 2015.
[29] P. Colegrove, S. Williams, Added Layer Manufacture, GB2491472, 2012.
[30] F. Martina, P.A. Colegrove, S.W. Williams, J. Meyer, Microstructure of Interpass Rolled Wire + Arc Additive Manufacturing Ti–6Al–4V Components, Metall. Mater. Trans. A (2015) 1.
[31] G.A. Sargent, K.T. Kinsel, A.L. Pilchak, A.A. Salem, S.L. Semiatin, Variant selection during cooling after beta annealing of Ti–6Al–4V ingot material, Metall. Mater. Trans. A 43 (2012) 3570–3585.
[32] P.S. Davies, An Investigation of Microstructure and Texture Evolution in the Near-α Titanium Alloy Timetal 834, University of Sheffield, 2009.
[33] P.S. Davies, B.P. Wynne, W.M. Rainforth, M.J. Thomas, P.L. Threadgill, Development of microstructure and crystallographic texture during stationary shoulder friction stir welding of Ti–6Al–4V, Metall. Mater. Trans. A 42 (2011) 2278–2289.
[34] M. Humbert, N. Gey, The calculation of a parent grain orientation from inherited variants for approximate (b.c.c.–h.c.p.) orientation relations, J. Appl. Crystallogr. 35 (2002) 401–405.
[35] N. Gey, M. Humbert, Specific analysis of EBSD data to study the texture inheritance due to the β → α phase transformation, J. Mater. Sci. 8 (2003) 1289–1294.
[36] T. Maitland, S. Sitzman, Scanning microscopy for nanotechnology: techniques and applications, Springer Science & Business Media, 2007.
[37] J.-Y. Kang, S.-J. Park, M.-B. Moon, Phase analysis on dual-phase steel using band slope of electron backscatter diffraction pattern, Microsc. Microanal. 19 (2013) 13–16.
[38] T.E. Buchheit, G.W. Wellman, C.C. Battaile, Investigating the limits of polycrystal plasticity modeling, Int. J. Plast. 21 (2005) 221–249.
[39] G. Deiter, Mechanical Metallurgy, third ed. McGraw-Hill Science, New York, 1986.
[40] U.F. Kocks, C.N. Tomé, H.-R. Wenk, Texture and Anisotropy: Preferred Orientations in Polycrystals and Their Effect on Materials Properties, Cambridge University Press, Cambridge, 2000.
[41] I. Dillamore, W. Roberts, Preferred orientation in wrought and annealed metals, Metall. Rev. (1965) 10.
[42] I. Lonardelli, N. Gey, H.-R. Wenk, M. Humbert, S.C. Vogel, L. Lutterotti, In situ observation of texture evolution during α → β and β → α phase transformations in titanium alloys investigated by neutron diffraction, Acta Mater. 55 (2007) 5718–5727.
[43] A.J.J. van Ginneken, W.G. Burgers, The habit plane of the zirconium transformation, Acta Crystallogr. 5 (1952) 548–549.
[44] G.C. Obasi, S. Birosca, J. Quinta da Fonseca, M. Preuss, Effect of β grain growth on variant selection and texture memory effect during α → β → α phase transformation in Ti–6Al–4V, Acta Mater. 60 (2012) 1048–1058.
[45] S. David, J. Vitek, Correlation between solidification parameters and weld microstructures, Int. Mater. Rev. (1989) 34.
[46] R. Ding, Z. Guo, Microstructural evolution of a Ti–6Al–4V alloy during β-phase processing: experimental and simulative investigations, Mater. Sci. Eng. A. 365 (2004) 172–179.
[47] J. Donoghue, A. Gholinia, J. Quinta da Fonseca, P.B. Prangnell, In-situ High Temperature EBSD Analysis of the Effect of aDeformation Step on the Alpha to Beta Transition in Additive Manufactured Ti–6Al–4V, TMS Titan, San Diago, 2015.
[48] R.K. Nalla, I. Altenberger, U. Noster, G.Y. Liu, B. Scholtes, R.O. Ritchie, On the influence of mechanical surface treatments-deep rolling and laser shock peening-on the fatigue behavior of Ti–6Al–4V at ambient and elevated temperatures, Mater. Sci. Eng. A 355 (2003) 216–230.